Dynamic Tire Friction Models for Combined Longitudinal and Lateral Vehicle Motion

Efstathios Velenis, Panagiotis Tsiotras, Carlos Canudas de Wit, Michel Sorine

Dynamic Tire Friction Models for Combined Longitudinal and Lateral Vehicle Motion

EFSTATHIOS VELENIS*, PANAGIOTIS TSIOTRAS*†
CARLOS CANUDAS-DE-WIT‡ and MICHEL SORINE§

SUMMARY

An extension to the LuGre dynamic friction model from longitudinal to longitudinal/lateral motion is developed in this paper. Application of this model to a tire yields a pair of partial differential equations that model the tire-road contact forces and aligning moment. A comparison of the steady-state behavior of the dynamic model with existing static tire friction models is presented. This comparison allows one to determine realistic values of the parameters for the new dynamic model. By the introduction of a set of mean states we reduce the partial differential equation to a lumped model governed by a set of three ordinary differential equations. Such a lumped form describes the aggregate effect of the friction forces and moments and it can be useful for control design and on-line estimation. A method to incorporate wheel rim rotation is also discussed. The proposed model is evaluated by comparing both its steady-state as well as its dynamic characteristics via a series of numerical simulations. The results of the simulations corroborate steady-state and dynamic/transient tire characteristics found in the literature.

1 INTRODUCTION

The problem of predicting the friction forces between the tire and the ground for wheeled vehicles is of enormous importance to the automotive industry. In the past several years, the problem of modelling and predicting tire friction has become an area of intense research in the automotive community [1, 2, 3]. Knowledge of the friction characteristics is necessary for the development of

*School of Aerospace Engineering, Georgia Institute of Technology, Atlanta, GA 30332-0150, USA, Tel: (404) 894-9526, Fax: (404) 894-2760, Email:{efstathios_velenis,p.tsiotras}@ae.gatech.edu

†Corresponding author.

‡Laboratoire d' Automatique de Grenoble, UMR CNRS 5528, ENSIEG-INPG, B.P.46, 38402, St. Martin d' Hères Cedex, FRANCE, Tel: +33-4-76826380, Fax: +33-4-76826388, Email:canudas@lag.ensieg.inpg.fr

§INRIA Rocquencourt, Domaine de Voluceau, B.P. 105, 78153 Le Chesnay Cedex, FRANCE, Tel: +33-1-39635648, Fax: +33-1-39635786, Email:michel.sorine@inria.fr

control systems such as the ABS, TCS, ESP, etc. which have enhanced safety and maneuverability of modern wheeled vehicles. Reliable characterization of the magnitude and direction of the friction force generated at the ground/tire interface may allow also in the future accurate control of autonomous vehicles travelling at high speeds and performing maneuvers by utilizing the maximum traction the tires can produce.

The most commonly used class of tire friction models in research and applications are the so-called "static" models. These models predict the friction force (magnitude and direction) as well as the aligning moment as a function of the slip for constant vehicle and tire angular velocity. The major representative of this class of models is "Pacejka's Magic Formula" [4, 5]. This is a semi-empirical model that uses a set of parameters to fit experimental data to a mathematical formula.

Existing steady-state models are typically based on slip and they suffer from singularities in low velocities. They also require redefinition of the slip ratios depending on acceleration/braking or forward/backward motion. Velocity dependence is also added only via ad-hoc methods. Most existing steady-state models represent rather artificial "curve fitting" procedures to experimental data and they do not interpret the physiological phenomena that give rise to the friction forces and moments. For a more in-depth discussion on the potential problems of steady-state models see [11].

Recently, a second class of tire friction models has been developed that capture the dynamic behavior of friction forces – the so-called "dynamic tire friction models" [6, 7, 8, 1, 9, 10, 3, 11]. In [6] dynamic models to handle the rate-independent hysteresis phenomena observed in practice were proposed. As an application to this work, a dynamic elastoplastic friction model was developed in [12]. This friction model was then applied to the longitudinal motion of a tire in [7] and extended to the longitudinal/lateral motion in [8, 1]. Slightly different in spirit is the work in [9] where a static map of relative velocity to friction and the dynamics of slip and slip angle development are used to predict tire friction forces, by taking into consideration the effects of length relaxation.

In this paper we extend the longitudinal LuGre friction model for tire-road contact, to the longitudinal/lateral motion of a wheeled vehicle. The LuGre tire friction model was initially introduced in [13] and was later corrected and improved upon in [2, 11]. The longitudinal LuGre tire friction model of [13, 11] was based on a dynamic visco-elastoplastic friction model for point contact introduced in [14]. Similar results have appeared in [8, 3, 10]. In [3], the coupling of the forces in different directions has been neglected, resulting in a set of two independent ordinary differential equations describing the deflection of the bristles at the contact patch in the longitudinal and lateral directions. In [10], the coupling of the forces in the longitudinal and lateral directions was taken into consideration in accordance to an extension of the static friction model for longitudinal/lateral motion in [4]. In [10], however the anisotropy of the friction characteristics in steady-state, and the rotation of the wheel rim were neglected. A more complete dynamic model is presented in [8]. This reference takes into consideration both the coupling of the friction forces in different directions and

the anisotropy of the friction characteristics in steady-state, as well as the effects of the wheel rim rotation. The model in [8] and the extension of the LuGre model proposed herein have both lumped forms resulting from a discretization of the distributed models. In [8] a discretization of the contact patch has been used, leading to a large number of states. On the contrary, in the present paper we follow an approach similar to [11] to obtain a lumped model with as a small number of ordinary differential equations (i.e., states) as possible. Such low-dimensional, lumped models are necessary for the development and implementation of *on-line* estimation and control algorithms [15, 16, 17]. In particular, in the context of the current paper we reserve the term "lumped model" for the mathematical description via a single ordinary differential equation along each direction, instead of a distributed model of an infinite number of states or a discretized distributed model with a large number of states. A lumped model is particularly appealing for developing control laws, as a large number of state variables complicates the control law design. It should be pointed out in this context that although highly-accurate, highly-specialized, (both static and dynamic) models do exist (and used widely in the automotive industry) that capture every aspect of the problem. These models predict friction forces and moments very accurately but they are not suitable for control analysis and design as their complexity makes such a proposition rather prohibitive.

In this paper we extend the LuGre tire friction model by taking into account all aspects neglected in [3, 10], that is, coupling of forces between longitudinal and lateral directions, tire anisotropy, and rim rotation. In addition, we provide a solid mathematical justification for the introduction of dynamic friction models based on fundamental physical properties of the friction forces, such as dissipativity and local maximality of the dissipation rate [18]. Finally, we also derive a lumped model which may be useful for control purposes.

The outline of the paper is as follows. In the first part of the paper we present a methodology that allows one to derive a static friction model for combined 2D (longitudinal, lateral and aligning moment) motion. Using this methodology, we derive a whole class of dynamic friction models. As a special case, we derive a LuGre friction model for 2D motion which reduces nicely to the longitudinal motion model of the 1D (longitudinal) case given in [11]. In the second part of the paper, using the same approach as in [13, 2, 11], we derive a distributed tire friction model for the longitudinal/lateral motion of the tire. We also look at the steady-state behavior of the new model and we compare it to the Pacejka tire model [4], to determine a set of realistic parameters for the former. Again, following the same approach as in the longitudinal motion model, we define a set of mean states and derive a reduced order lumped model. In the last part of the paper we investigate the effect of the wheel rim rotation on both the distributed and the lumped models. Finally, the transient, dynamic response of the model is evaluated with respect to results found in the literature.

2 A TWO-DIMENSIONAL COULOMB FRICTION MODEL

Recall that the Coulomb friction model for the longitudinal motion of a body, with velocity v_r relative to the contact surface, provides the friction force coefficient by

$$\mu(v_r) = \begin{cases} -\mu_k & \text{for } v_r > 0, \\ [-\mu_s, \mu_s] & \text{for } v_r = 0, \\ \mu_k & \text{for } v_r < 0 \end{cases} \tag{1}$$

where μ_k is the kinetic and μ_s is the static friction coefficient. The friction force is given by $F = \mu F_n$ where F_n is the normal load. Typically, $\mu_s \geq \mu_k > 0$. Consider now the simple case when $\mu_s = \mu_k$. We can derive the same model as in (1) by applying the Maximal Dissipation Rate Principle [18] to the following set of admissible friction coefficients

$$\mathcal{C} = \{\mu \in \mathbb{R} : |\mu_k^{-1}\mu| \leq 1\} \ . \tag{2}$$

Notice that if $\mu_k = \mu_s$ then $\mu \in [-\mu_k, \mu_k]$, which is equivalent to the condition $\mu \in \mathcal{C}$. A dissipation rate is the product of the friction force with the relative velocity

$$D(v_r, \mu) := -\mu F_n v_r,$$

and the Coulomb friction force coefficient μ^* is the one in the admissible set that maximizes the dissipation rate, i.e.,

$$\mu^* = \text{argmax}_{\mu \in \mathcal{C}}[-\mu F_n v_r(t)], \quad \forall v_r, \forall t > 0. \tag{3}$$

It is easy to prove the following result.

Theorem 1 ([8]) The solution to (2), (3) is given by

$$\mu^* = -\text{sign}(v_r)\mu_k \tag{4}$$

and the maximum dissipation rate is

$$D(v_r, \mu^*) = -\mu^* F_n v_r = \mu_k F_n |v_r| \tag{5}$$

Now consider the case of combined longitudinal/lateral motion of a body with velocities v_{rx}, v_{ry} relative to the contact surface along the longitudinal and lateral directions, respectively. Let the velocity vector $v_r := \begin{bmatrix} v_{rx} & v_{ry} \end{bmatrix}^T$ and let

$$M_k := \begin{bmatrix} \mu_{kx} & 0 \\ 0 & \mu_{ky} \end{bmatrix} > 0 \tag{6}$$

be the matrix of kinetic friction coefficients, with μ_{kx} and μ_{ky} the friction coefficients for longitudinal motion along the x and y directions, respectively. The two coefficients can be equal for a completely symmetric situation. In general, they

are different since friction characteristics change with the direction of motion [8].

In analogy to (2), the set of admissible friction coefficient vectors $\mu = \begin{bmatrix} \mu_x & \mu_y \end{bmatrix}^T$ may now be defined as

$$\mathcal{C} = \{\mu \in \mathbb{R}^2 : \|M_k^{-1}\mu\| \leq 1\} \ . \tag{7}$$

The Coulomb friction force coefficient will again be the one from the admissible set that maximizes the dissipation rate. Thus,

$$\mu^* = \text{argmax}_{\mu \in \mathcal{C}}[-F_n \mu^T v_r(t)], \quad \forall v_r, \forall t > 0. \tag{8}$$

The following result can be found in [8].

Theorem 2 ([8]) The solution to (7), (8) is given by

$$\mu^* = -\frac{M_k^2 v_r}{\|M_k v_r\|} \tag{9}$$

and the maximum dissipation rate is

$$D(v_r, \mu^*) = -F_n \mu^{*T} v_r = F_n \|M_k v_r\| \tag{10}$$

Proof For $\mu \in \mathcal{C}$ and by the Cauchy - Schwarz inequality the following holds

$$-\mu^T M_k^{-1} M_k v_r \leq |\mu^T M_k^{-1} M_k v_r| \leq \|\mu^T M_k^{-1}\| \|M_k v_r\| \leq \|M_k v_r\|$$

which implies

$$\begin{aligned} \|M_k v_r\| &\geq -\mu^T M_k^{-1} M_k v_r \\ \frac{1}{\|M_k v_r\|} v_r^T M_k^T M_k v_r &\geq -\mu^T v_r \\ \frac{F_n}{\|M_k v_r\|} v_r^T M_k^2 v_r &\geq -F_n \mu^T v_r \\ -F_n \mu^{*T} v_r &\geq -F_n \mu^T v_r, \quad \forall \mu \in \mathcal{C} \end{aligned}$$

Thus, we have that $D(v_r, \mu^*) = -F_n \mu^{*T} v_r = F_n \|M_k v_r\| \geq D(v_r, \mu)$ for all $\mu \in \mathcal{C}$. □

Observe that $\mu \in \mathcal{C}$ does not imply dissipativity of the friction force. Actually, $\mu \in \mathcal{C}$ implies $-\mu \in \mathcal{C}$ and if $F_n \mu^T v_r \geq 0$ then $-F_n \mu^T v_r \leq 0$. On the other hand, conditions (2), (3) or (7), (8) together imply dissipativity of the friction force. Since $0 \in \mathcal{C}$, it follows that $F_n \mu^{*T} v_r \leq 0$.

The set $\mathcal{C}$ provides bounds for the friction forces and also a coupling between the forces in different directions; see Fig. 1. In the case where $\mu_{kx} = \mu_{ky} = \mu_k$ then $\mu \in \mathcal{C} \Leftrightarrow \|\mu\| \leq \mu_k$ which is a circle in the $\mu_x - \mu_y$ plane.

Observe that for μ^* from (9) we have that $\|M_k^{-1}\mu^*\| = 1$ which means that the predicted Coulomb friction coefficient μ^* always lies on the boundary of the

friction ellipse (Fig 1). Thus, the set of admissible friction coefficients can be rewritten as

$$\mathcal{C} = \{\mu \in \mathbb{R}^2 : \|M_k^{-1}\mu\| \leq \|M_k^{-1}\mu^*\|\} \ . \tag{11}$$

Finally, observe that the maximization of the dissipation rate was done for the case where $v_r \neq 0$. Obviously when $v_r = 0$ the dissipation rate $D(v_r, \mu) = 0$ regardless of the value of μ. In this case the friction coefficient is bounded by the static friction coefficients $\|M_s^{-1}\mu\| \leq 1$ where

$$M_s = \begin{bmatrix} \mu_{sx} & 0 \\ 0 & \mu_{sy} \end{bmatrix} > 0 \ , \tag{12}$$

is the matrix of static friction coefficients.

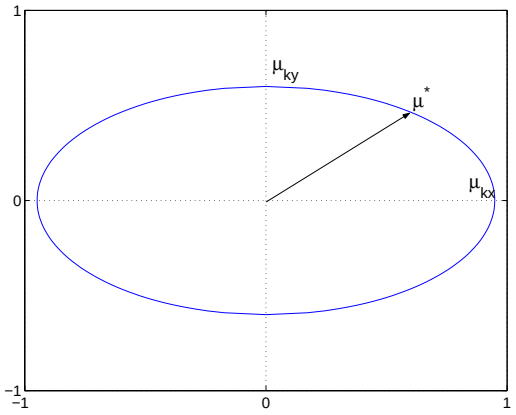

Figure 1: Set $\mathcal{C}$ of admissible coefficients for the two-dimensional Coulomb case.

3 A CLASS OF TWO-DIMENSIONAL DYNAMIC FRICTION MODELS

Using the set $\mathcal{C}$ of admissible friction coefficients and the Maximal Dissipation Rate Principle [8, 18], dynamic friction models for the 2D motion (longitudinal and lateral) of a body are derived. In this section we summarize the results of [8, 18] which will be useful in our developments. Dynamic models assume that friction is generated due to the interaction forces between microscopic bristles at the contact area; see Fig. 2.

Most importantly, dynamic friction models can capture the Stribeck effect [14], according to which the steady-state friction coefficient decreases monotonically with v_r and the kinetic friction coefficients μ_{kx} and μ_{ky} provide bounds for the

friction coefficient components only asymptotically, i.e. as $\|v_r\| \to \infty$. To this end, let M_k as in (6) be the matrix of asymptotic friction coefficients and let

$$K = F_n \begin{bmatrix} \sigma_{0x} & 0 \\ 0 & \sigma_{0y} \end{bmatrix} > 0 \tag{13}$$

be the matrix of stiffnesses of the bristles. Denote by u the relative deformation of a bristle at the contact area of the body and by $F = \mu F_n$ the associated force. Consider the elastic and plastic deformations $u_e = -F_n K^{-1}\mu$ and $u_p = u - u_e$ respectively, as shown in Fig. 2. Dissipation depends only on the plastic deformation. Therefore, $D(\dot{u}_p, \mu) = -F_n \mu^T \dot{u}_p$ is the dissipation rate that must be positive and maximal. The friction coefficient μ^* is then given by the following

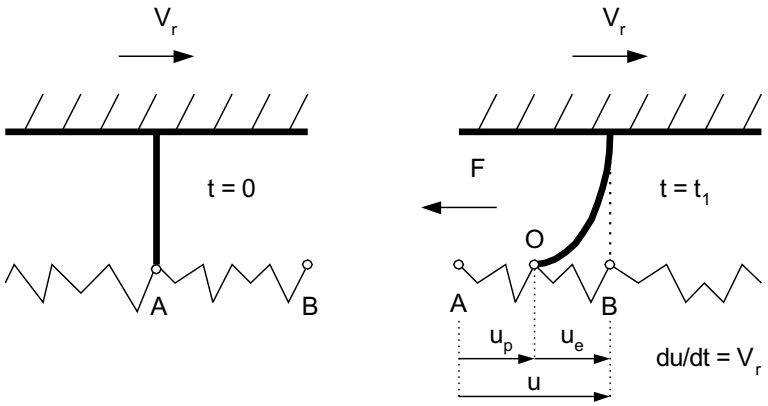

Figure 2: Microscopic view of dynamics of friction.

Quasi-Variational Inequality (QVI) [8]

$$D(\dot{u}_p, \mu^*) \geq D(\dot{u}_p, \mu) \Rightarrow -(\dot{u} + F_n K^{-1}\dot{\mu^*})^T(\mu^* - \mu) \geq 0 \tag{14}$$

$$\forall\ \mu \in \mathcal{C} = \{\mu \in \mathbb{R}^2 : \|M_k^{-1}\mu\| \leq \|M_k^{-1}\mu^*\|\}. \tag{15}$$

Observe that, in analogy to the Coulomb model of the previous section, the solution μ^* of the friction model is the one in the admissible set $\mathcal{C}$ that maximizes the dissipation rate. Observe also that we use the expression (11) for the set $\mathcal{C}$ which provides the coupling between the friction coefficient components. One cannot use here (7) because this expression, in addition to the coupling of the components, implies that the friction coefficient components are bounded by the Coulomb friction coefficients at all time, which contradicts the Stribeck effect (see previous discussion).
The QVI (14)-(15) has many solutions. In [8, 18] a class of solutions is proposed, generating a class of dynamic friction models as follows

Theorem 3 ([8]) Any solution μ^* of

$$-F_n K^{-1}\dot{\mu^*} - \lambda(u, \dot{u}, \mu^*) M_k^{-2}\mu^* = \dot{u} \tag{16}$$

where $\mu^*(0) = \mu_0$, satisfies (14)-(15) for all $\lambda(u, \dot{u}, \mu^*) \geq 0$.

Proof Denote $\dot{u}_p = \dot{u} - F_n K^{-1} \dot{\mu}$. For $\mu \in \mathcal{C}$ and by the Cauchy-Schwarz inequality the following holds

$$-\dot{u}_p^T \mu \leq |\dot{u}_p^T M_k M_k^{-1} \mu| \leq \|M_k \dot{u}_p\| \|M_k^{-1} \mu\| \leq \|M_k \dot{u}_p\| \|M_k^{-1} \mu^*\| \tag{17}$$

Note that (16) implies that

$$\begin{aligned} -F_n K^{-1} \dot{\mu}^* - \lambda(u, \dot{u}, \mu^*) M_k^{-2} \mu^* &= \dot{u} \\ \dot{u} + F_n K^{-1} \dot{\mu}^* &= -\lambda(u, \dot{u}, \mu^*) M_k^{-2} \mu^* \\ M_k \dot{u}_p &= -\lambda(u, \dot{u}, \mu^*) M_k^{-1} \mu^* \end{aligned}$$

with $\lambda(u, \dot{u}, \mu^*) \geq 0$. It follows that (17) implies that

$$-\dot{u}_p^T \mu \leq -\dot{u}_p^T M_k M_k^{-1} \mu^* = -\dot{u}_p^T \mu^*$$

Thus we have that $D(\dot{u}_p, \mu^*) \geq D(\dot{u}_p, \mu)$ for all $\mu \in \mathcal{C}$. □

Several multi-dimensional dynamic friction models can be derived using (16) by choosing different scalar functions $\lambda(u, \dot{u}, \mu^*)$. The LuGre model [18] corresponds to the specific choice

$$\lambda(u, \dot{u}, \mu^*) = \lambda(\dot{u}) := \frac{\|M_k^2 \dot{u}\|}{g(\dot{u})} \tag{18}$$

with

$$g(\dot{u}) := \frac{\|M_k^2 \dot{u}\|}{\|M_k \dot{u}\|} + \tilde{g}(\|M_k \dot{u}\|) \tag{19}$$

where $\tilde{g}(\|M_k \dot{u}\|) \to 0$ when $\dot{u} \to +\infty$. Note that we wish a model which asymptotically (as $\dot{u} \to +\infty$) approaches the Coulomb model (9) presented in the previous section. Therefore, the function $g(\dot{u})$ characterizes the steady-state of our dynamic model. In particular, for $\dot{u} \to +\infty$, (18) and (19) lead to

$$g(\dot{u}) \to \frac{\|M_k^2 \dot{u}\|}{\|M_k \dot{u}\|} \quad \text{and} \quad \lambda(\dot{u}) \to \|M_k \dot{u}\| \tag{20}$$

The steady-state friction coefficient is found by setting $\dot{\mu}^* = 0$ in (16)

$$\mu^{*\text{ss}} \to -\frac{M_k^2 \dot{u}}{\lambda(\dot{u})} = -\frac{M_k^2 \dot{u}}{\|M_k \dot{u}\|} \tag{21}$$

exactly as in (9). This justifies the choice of the particular $\lambda(u, \dot{u}, \mu^*)$ in (18).

4 LUGRE FRICTION MODEL FOR 2D MOTION

The LuGre friction model proposed in the previous section assumes that the friction is proportional only to the deflection (elastic deformation u_e) of the bristles at the contact point. Henceforth, we will refer to u_e as the internal friction state and we will denote by z. In fact, it has already been assumed that $\mu = -(K/F_n)z$ and thus $\dot{\mu} = -(K/F_n)\dot{z}$. In order to include the dependence of the friction on the rate of z and the relative velocity at the point of contact $\dot{u}$, i.e., in order to include the damping and the viscous friction effects , we rewrite equation (16) in terms of the internal friction state z. We then have [14]

$$\dot{z} = \dot{u} - \lambda(u, \dot{u}, z) M_k^{-2} \frac{K}{F_n} z \tag{22}$$

where for the LuGre model the function $\lambda(u, \dot{u}, z)$ is given in (18). Finally, we choose $g(\dot{u})$ and $\tilde{g}(\dot{u})$ to be able to recover the LuGre friction model of [14] for longitudinal motion. To this end, we choose

$$g(\dot{u}) = \frac{\|M_k^2 \dot{u}\|}{\|M_k \dot{u}\|} + \left(\frac{\|M_s^2 \dot{u}\|}{\|M_s \dot{u}\|} - \frac{\|M_k^2 \dot{u}\|}{\|M_k \dot{u}\|} \right) e^{-\left(\frac{\|\dot{u}\|}{v_s}\right)^{\gamma}} \tag{23}$$

where M_s is the matrix of static friction coefficients as in (12) and v_s and γ are parameters used to achieve desirable steady-state behavior [11, 14]. Finally, the friction coefficient vector, including damping for z and a viscous friction component, is given by

$$\mu = -\begin{bmatrix} \sigma_{0x} & 0 \\ 0 & \sigma_{0y} \end{bmatrix} z - \begin{bmatrix} \sigma_{1x} & 0 \\ 0 & \sigma_{1y} \end{bmatrix} \dot{z} - \begin{bmatrix} \sigma_{2x} & 0 \\ 0 & \sigma_{2y} \end{bmatrix} \dot{u}. \tag{24}$$

Equations (18),(22), (23) and (24) represent the LuGre friction model for combined longitudinal/lateral motion. This model reduces nicely to the longitudinal motion model of [14] in the 1D case.

To write the previous equations in terms of the x and y components let

$$z = \begin{bmatrix} z_x \\ z_y \end{bmatrix}, \quad \mu = \begin{bmatrix} \mu_x \\ \mu_y \end{bmatrix} \quad \text{and} \quad \dot{u} = v_r = \begin{bmatrix} v_{rx} \\ v_{ry} \end{bmatrix} \tag{25}$$

The proposed friction model is then written as follows

$$\dot{z}_i = v_{ri} - C_{0i}(v_r) z_i \tag{26a}$$

$$\mu_i = -\sigma_{0i} z_i - \sigma_{1i} \dot{z}_i - \sigma_{2i} v_{ri} \tag{26b}$$

where,

$$C_{0i}(v_r) = \frac{\lambda(v_r)\sigma_{0i}}{\mu_{ki}^2}, \qquad i = x, y \tag{27}$$

The scalar function $\lambda(v_r)$ is given by (18) and the function $g(v_r)$ by (23). Observe that the forces in the x and y directions are coupled due to $\lambda(v_r)$. This is consistent with the two-dimensional Coulomb friction model in (9) and Fig. 1.

5 TWO-DIMENSIONAL LUGRE TIRE FRICTION MODEL

5.1 Distributed Model

In this section we apply the LuGre friction model for 2D motion, in order to derive a model for the tire-road contact forces and moments due to friction. We follow an approach similar to that in [13, 11]. To this end, we assume that the contact patch of the tire (the area of contact with the road) is rectangular (Fig. 3). We divide the contact patch into infinitesimal elements. For each element we apply the point LuGre model for 2D motion of equations (26)-(27). In order to find the total forces and moments we then integrate the forces of each element along the patch. It should be mentioned that although we will keep referring to this friction model as 2D model, it will be in fact a 3-dof model since not only the longitudinal and lateral forces but the aligning moment will be captured as well.

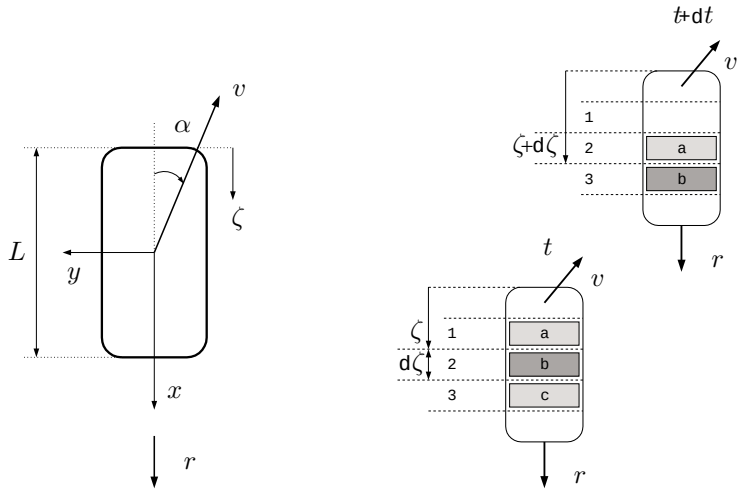

Figure 3: Frames of reference and velocities at the contact patch.

To this end, let v denote the velocity of the vehicle and let ω denote the angular velocity of the wheel of radius r. Let α be the slip angle of the wheel, that is, the angle between the velocity vector and the x (longitudinal) body axis of the tire. Let us also assume, for the time being, that the wheel rim is not rotating, i.e., the steering angle is constant. In general, the velocity of the tire has components in both x and y axes. The relative velocity components of the elements in the contact patch with respect to the ground are

$$v_{rx} = \omega r - v\cos(\alpha) \tag{28a}$$

$$v_{ry} = -v\sin(\alpha) \tag{28b}$$

Considering a frame fixed on the contact patch, we observe that the tire elements move only along the length of the patch (ζ direction). For each tire element on

the patch we can compute the friction using the LuGre model of the previous section. The internal friction states z_i $(i = x, y)$ now become functions of both time t and the position of the element on the patch ζ.
Let $z_i(t, \zeta)$ denote the deflections of the patch element along x and y directions respectively, located at the point ζ with respect to the patch frame at a certain time t (element b in Fig. 3). Consider the total deflection of this element between two time instances t and $t+\mathrm{d}t$. Since during the time interval $\mathrm{d}t$ the element has moved to the location $\zeta + \mathrm{d}\zeta$, and using (26) we have that the total deflections $\mathrm{d}z_i$ are

$$\mathrm{d}z_i = z_i(t + \mathrm{d}t, \zeta + \mathrm{d}\zeta) - z_i(t, \zeta) = (v_{ri} - C_{0i}(v_r)z_i(t, \zeta))\mathrm{d}t, \quad i = x, y$$

Since $\mathrm{d}z_i = \frac{\partial z_i}{\partial \zeta}\mathrm{d}\zeta + \frac{\partial z_i}{\partial t}\mathrm{d}t$ and using the fact that $\mathrm{d}\zeta/\mathrm{d}t = |\omega r|$ the friction model is summarized by the following equations

$$\frac{\mathrm{d}z_i(t, \zeta)}{\mathrm{d}t} = \frac{\partial z_i(t, \zeta)}{\partial t} + \frac{\partial z_i(t, \zeta)}{\partial \zeta}|\omega r| = v_{ri} - C_{0i}(v_r)z_i(t, \zeta) \tag{29a}$$

$$\mu_i(t, \zeta) = -\sigma_{0i}z_i(t, \zeta) - \sigma_{1i}\frac{\partial z_i(t, \zeta)}{\partial t} - \sigma_{2i}v_{ri}, \tag{29b}$$

where $i = x, y$. The total forces along the x and y directions are computed from

$$F_i(t) = \int_0^L \mu_i(t, \zeta)f_n(\zeta)\mathrm{d}\zeta, \quad i = x, y \tag{30}$$

where $f_n(\zeta)$ is the normal load distribution (force per unit length) along the contact patch and L is the length of the patch. The force distribution along the y direction also results into a moment about the center of the patch (aligning torque) given by

$$M_z(t) = -\int_0^L \mu_y(t, \zeta)f_n(\zeta)\left(\frac{L}{2} - \zeta\right)\mathrm{d}\zeta \tag{31}$$

To evaluate this distributed model we compare it against other tire models. In particular, we have made comparison with Pacejka's Magic Formula (MF) model [4]. This tire mode is used widely in the automotive industry and captures accurately actual tire characteristics under steady-state conditions (i.e., for constant vehicle speed and wheel angular velocity). For consistency, in the following we compare the forces predicted by the previous distributed model with the MF model under such steady-state conditions.

5.2 Steady-State Conditions

The steady-state time characteristics of the model (29) are obtained by setting $\frac{\partial z(t,\zeta)}{\partial t} = 0$, and by imposing that the velocities v and ω (and hence v_r) are constant. In this case, the pde in (29a) becomes

$$\frac{\partial z_i(t, \zeta)}{\partial \zeta} = \frac{1}{|\omega r|}\left(v_{ri} - C_{0i}(v_r)z_i(t, \zeta)\right), \quad i = x, y, \quad \omega \neq 0 \tag{32}$$

For $\omega = 0$ equation (29a) reduces to equation (26a) of the point contact LuGre model for $\omega = 0$. This is in agreement with the physics of the problem, as in this case the tire is a body in pure translation and its dynamics should coincide with those of a point-contact dry friction model, which are given by equation (26a).
Enforcing the boundary condition $z_i(t,0) = 0$ (no deflection at the entry point of the patch) and the steady-state conditions of constant v and ω, we may integrate (32) to obtain

$$z_i^{\text{ss}}(\zeta) = C_{1i}\left(1 - e^{-\frac{\zeta}{C_{2i}}}\right), \quad i = x, y \tag{33}$$

where,

$$C_{1i} := \frac{v_{ri}\mu_{ki}^2}{\lambda(v_r)\sigma_{0i}}, \quad C_{2i} := \frac{|\omega r|}{C_{0i}(v_r)}, \quad i = x, y \tag{34}$$

We can now compute the steady-state expressions for the forces and the alignment torque using (30) and (31). In particular, we have

$$F_i^{\text{ss}} = -\int_0^L \left(\sigma_{0i} z_i^{\text{ss}}(\zeta) + \sigma_{2i} v_{ri}\right) f_n(\zeta) \mathrm{d}\zeta \ , \quad i = x, y \tag{35}$$

$$M_z^{\text{ss}} = \int_0^L \left(\sigma_{0y} z_y^{\text{ss}}(\zeta) + \sigma_{2y} v_{ry}\right) f_n(\zeta) \left(\frac{L}{2} - \zeta\right) \mathrm{d}\zeta \tag{36}$$

Before we proceed with our analysis, a few words about the normal load distribution f_n are in order. One may be tempted to assume uniform load distribution i.e. $f_n = \text{const}$. This is not a realistic assumption, because the uniform load distribution does not satisfy the natural boundary conditions of zero normal load at the edges of the patch. In addition, the uniform load distribution would lead to an aligning torque that does not change sign at higher lateral slip angles, as observed in practice. To this end, we adopt a more realistic (but still quit simple to integrate) load distribution, namely, a trapezoidal distribution, as proposed by Deur et al in [10]. In this case, the function f_n is given by

$$f_n(\zeta) = \begin{cases} \alpha_1 \zeta & \text{for } \ 0 \le \zeta \le \zeta_L, \\ f_{\max} & \text{for } \ \zeta_L \le \zeta \le \zeta_R, \\ \alpha_2 \zeta + \beta_2 & \text{for } \ \zeta_R \le \zeta \le L \end{cases} \tag{37}$$

with $f_{\max}$ being the maximum value of the normal load distribution; see Fig. 4. Here ζ_L and ζ_R are parameters which determine the position of the linear and constant portions of the distribution, and

$$\alpha_1 = \frac{f_{\max}}{\zeta_L}, \quad \alpha_2 = -\frac{f_{\max}}{L - \zeta_R}, \quad \beta_2 = \frac{L f_{\max}}{L - \zeta_R} \ . \tag{38}$$

The total normal force is therefore,

$$F_n = \int_0^L f_n(\zeta) \mathrm{d}\zeta = \frac{L + \zeta_R - \zeta_L}{2} f_{\max} \ . \tag{39}$$

Note that the proposed normal load distribution (Fig. 4) satisfies the associated boundary conditions and allows the effects of the pneumatic trail to appear. It is quite simple to integrate leading to a relatively simple average lumped model that we discuss later on in the paper. A more realistic expression for the normal load can of course be used in equations (30) and (31), thus resulting in a higher fidelity model. However, such higher order normal distributions would necessarily increase the complexity of the model.

Next, we calculate the expressions (35) and (36) using $f_n(\zeta)$ from (37). The explicit expressions for the steady-state forces and the aligning moment are given in the Appendix.

Using the definitions of the longitudinal slip, for the braking and accelerating cases [3]

$$s := \begin{cases} \dfrac{v_{rx}}{\omega r}, & \text{for } \; v\cos(\alpha) < \omega r, \\ -\dfrac{v_{rx}}{v\cos(\alpha)}, & \text{for } \; \omega r \leq v\cos(\alpha) \end{cases} \tag{40}$$

we construct the steady-state s–$F_x^{\text{ss}}, F_y^{\text{ss}}$ and α–M_z^{ss} plots shown in Fig. 5. Steady-state plots of longitudinal and lateral forces with longitudinal slip rate, and for different constant values of lateral slip α, plots of longitudinal and lateral forces with lateral slip and for different constant values of longitudinal slip, as well as the friction ellipse plots are shown in Fig. 6 and Fig. 7. These figures are in qualitative agreement with similar curves found in the literature [4, 19].

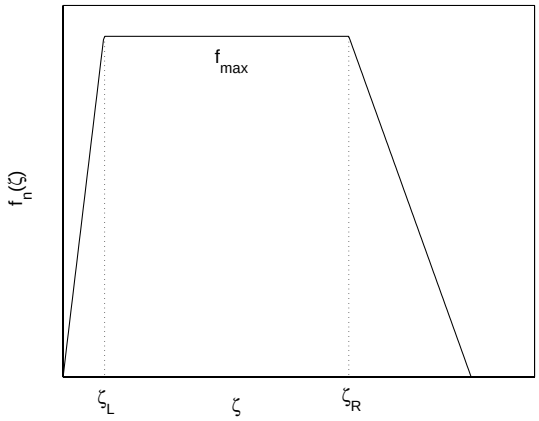

Figure 4: Trapezoidal load distribution.

5.3 Parameter Fitting

In order to use the model (29) in practice several parameters need to be identified. In this section, we propose a method to identify the unknown parameters

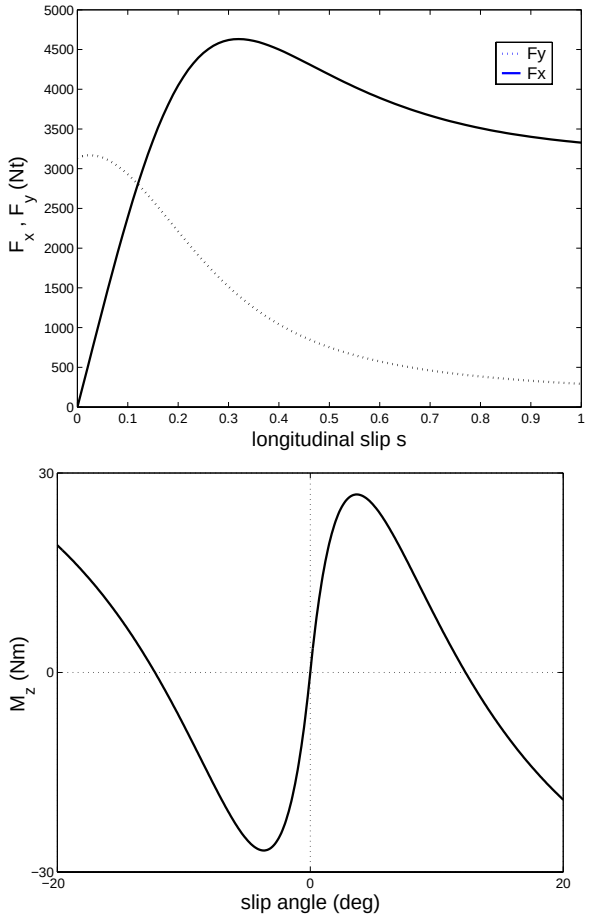

Figure 5: Steady-state forces $F_x^{\text{ss}}, F_y^{\text{ss}}$ and aligning moment M_z^{ss}.

in (29) by comparing the steady-state characteristics of the model to steady-state data. Such steady-state data are easily obtainable by experiments and can be readily found in the literature [4]. In particular, we compare the forces and aligning moment predicted by the steady-state expressions (33)-(36) to the forces and moment generate by the MF using the MF parameters shown in Table 1. These parameters have been identified in [4] to fit experimental data.

The identification of the parameters for the LuGre tire model was done by fitting the plots generated by the steady-state expressions (35) and (36) to the MF plots with the above parameters. The curve fitting was done using the `lsqnonlin` command in MATLAB which solves an associated nonlinear least squares problem. The data used in generating the plots for the MF corresponded to cases of pure braking and pure cornering, i.e. there were no lateral forces and aligning moment during braking and no longitudinal forces during cornering.

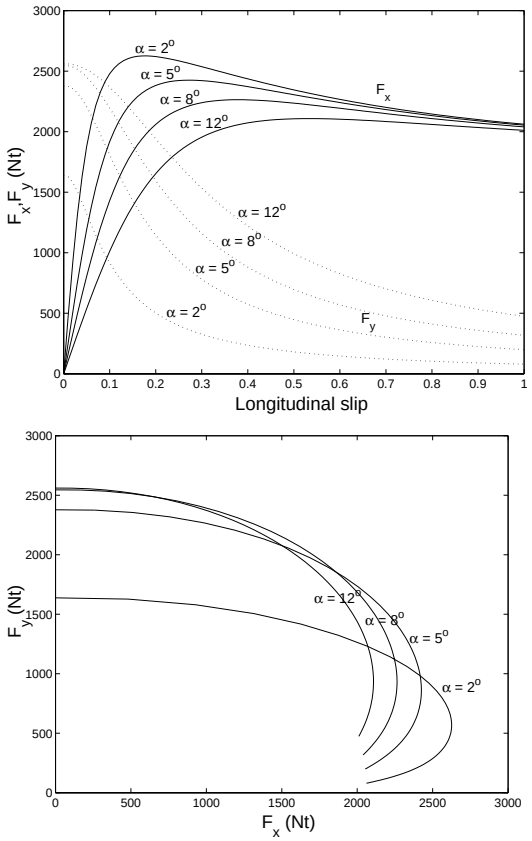

Figure 6: Steady-state forces for several constant values of the slip angle.

Thus, the parameters $\sigma_{0x}, \mu_{kx}, \mu_{sx}, \sigma_{2x}$ were identified by fitting the longitudinal friction forces plots, the parameters $\sigma_{0y}, \mu_{ky}, \mu_{sy}, \sigma_{2y}$ were identified by fitting the lateral friction forces and aligning moment plots simultaneously while the parameters $\gamma, L, \zeta_L, \zeta_R$ and v_s were identified by trial and error in order to achieve best overall fitting of all longitudinal/lateral forces and aligning moment plots.

The identified parameters are given in Table 2. The results are shown in Fig. 8. The F_x plot shown at the top of Fig. 8 is for pure braking i.e., longitudinal motion with $\alpha = 0$ and vehicle speed 60 km/h. The F_y and M_z plots are for pure cornering i.e., $s = 0$ and vehicle speed 70 km/h. In all cases the normal load was $F_n = 2000$ N. Even for the relatively simple trapezoidal load distribution the agreement between the curves in Fig. 8 is very good, especially for the forces. Some discrepancy exists in the plot of the aligning moment. This can be explained as follows: the MF model for pure cornering provides two independent equations for the lateral forces and aligning moment and has thus

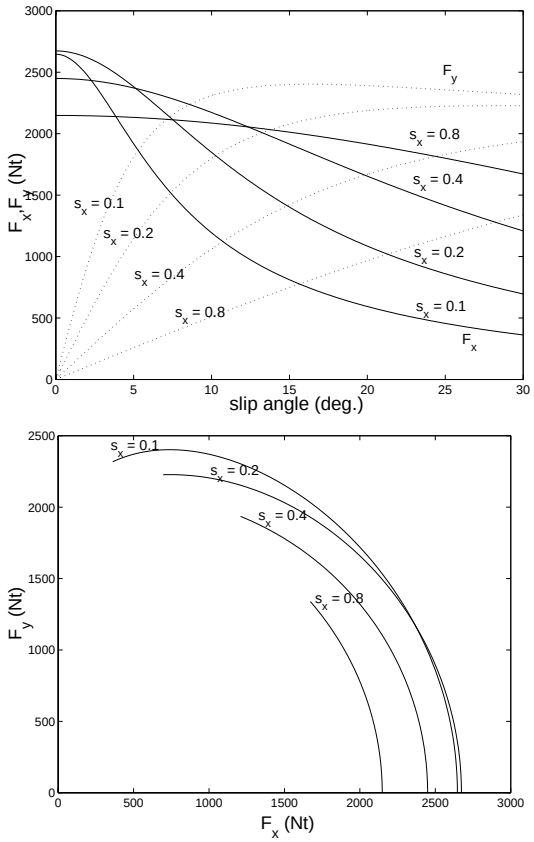

Figure 7: Steady-State forces for several constant values of the longitudinal slip.

enough freedom to fit both sets of experimental data. This is somewhat artificial, since it is clear from the physics of the problem that the lateral forces and the aligning moment are related. The LuGre dynamic model naturally captures this coupling. The reason for the slight discrepancy between the aligning moments at the bottom of Fig. 8 is due to the simple normal load distribution used in this example. A more realistic normal force distribution can be used if a better fitting for the aligning moment is desired.

Table 1: Parameters for the Magic Formula; taken from [4].

Parameters	B	C	D	E
F_x	0.178	1.55	2193	0.432
F_y	0.244	1.5	1936	-0.132
M_z	0.247	2.56	-15.53	-3.92

Table 2: Identified Parameters.

σ_{0x} (1/m)	μ_{kx}	μ_{sx}	$\sigma_{2x,y}$ (sec/m)
555	0.7516	1.35	0
σ_{0y} (1/m)	μ_{ky}	μ_{sy}	γ
470	0.75	1.4	1
L (m)	ζ_L/L	ζ_R/L	v_s (m/sec)
0.15	0.02	0.77	3.96

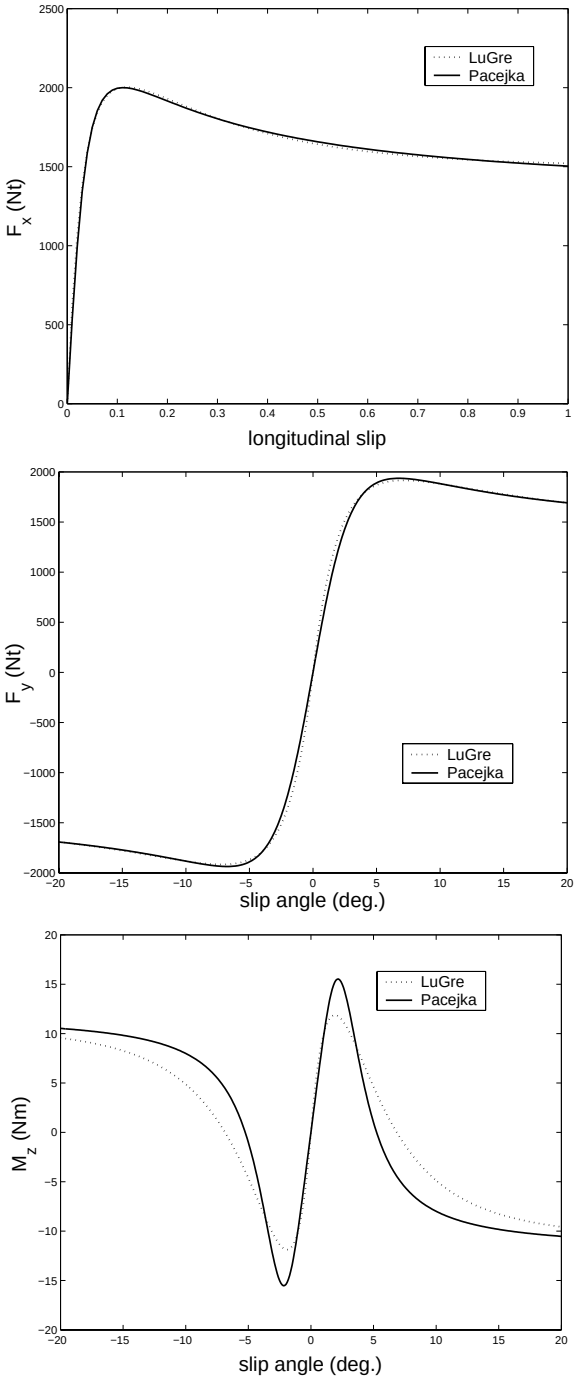

Figure 8: Comparison between LuGre and Pacejka (Magic Formula) models. The values of the parameters for the Magic Formula were taken from [4] and correspond to experimental data.

5.4 Average Lumped Model

The distributed model (29) may not be easy to use for analysis and – most importantly – control design. In this section, we develop a lumped model, described by a single ordinary differential equation, which captures the "average" behavior of the internal friction states. It is used to approximate the longitudinal and lateral forces as well as the aligning torque as a function of these "average states," at least at steady-state. The approach used in this section mimics the one used in Refs. [13, 11] for the longitudinal case.

Recall the expressions for the longitudinal and lateral forces at the contact patch. According to (30) we have

$$F_i(t) = -\int_0^L \left(\sigma_{0i} z_i(t,\zeta) + \sigma_{1i}\frac{\partial z_i(t,\zeta)}{\partial t} + \sigma_{2i} v_{ri}\right) f_n(\zeta)\mathrm{d}\zeta \ , \quad i = x, y.$$

Define now, as in [11], the weighted mean internal friction states $\bar{z}_i$ along the x and y directions as follows

$$\bar{z}_i(t) := \frac{1}{F_n}\int_0^L z_i(t,\zeta) f_n(\zeta)\mathrm{d}\zeta, \quad i = x, y. \tag{41}$$

We thus we have that

$$\frac{\mathrm{d}\bar{z}_i(t)}{\mathrm{d}t} = \frac{1}{F_n}\int_0^L \frac{\partial z_i(t,\zeta)}{\partial t} f_n(\zeta)\mathrm{d}\zeta, \quad i = x, y. \tag{42}$$

The total friction force can then be written in terms of the mean states $\bar{z}_i$ as follows,

$$F_i(t) = -F_n\left(\sigma_{0i}\bar{z}_i(t) + \sigma_{1i}\dot{\bar{z}}_i(t) + \sigma_{2i} v_{ri}\right). \tag{43}$$

To complete the model we need to determine the dynamics of the mean states. To this end, from (42) and (29a) we have that

$$\begin{aligned}
\dot{\bar{z}}_i(t) &= \frac{1}{F_n}\int_0^L \left(v_{ri} - C_{0i}(v_r) z_i(t,\zeta) - \frac{\partial z_i(t,\zeta)}{\partial \zeta}|\omega r|\right) f_n(\zeta)\mathrm{d}\zeta \\
&= v_{ri} - C_{0i}(v_r)\bar{z}_i(t) - \frac{|\omega r|}{F_n}\left[z_i(t,\zeta) f_n(\zeta)\right]_0^L + \frac{|\omega r|}{F_n}\int_0^L z_i(t,\zeta)\frac{\partial f_n(\zeta)}{\partial \zeta}\mathrm{d}\zeta \\
&= v_{ri} - C_{0i}(v_r)\bar{z}_i(t) - \kappa_i(t)|\omega r|\bar{z}_i(t) \ , \quad i = x, y
\end{aligned} \tag{44}$$

where,

$$\kappa_i(t) := -\frac{\int_0^L z_i(t,\zeta) f_n'(\zeta)\mathrm{d}\zeta}{\int_0^L z_i(t,\zeta) f_n(\zeta)\mathrm{d}\zeta} \ , \quad i = x, y \tag{45}$$

and where $(|\omega r|/F_n)\left[z_i(t,\zeta) f_n(\zeta)\right]_0^L = 0$ because of the assumed normal load distribution in (37). Thus, the average lumped model for the friction forces is

summarized by the following equations.

$$\dot{\bar{z}}_i(t) = v_{ri} - C_{0i}(v_r)\bar{z}_i(t) - \kappa_i(t)|\omega r|\bar{z}_i(t) \tag{46}$$

$$\bar{F}_i(t) = -F_n(\sigma_{0i}\bar{z}_i(t) + \sigma_{1i}\dot{\bar{z}}_i(t) + \sigma_{2i}v_{ri}), \quad i = x, y. \tag{47}$$

Using the definition for $\kappa_i(t)$ from (45) the friction forces of the lumped model $\bar{F}_i$ from (47) are equal to the forces F_i calculated from the distributed model (30). However, the calculation of $\kappa_i(t)$ from (45) requires the solution $z_i(t,\zeta)$ from the partial differential equation (29a) of the distributed model. In order to derive a lumped model which is independent from the distributed model we approximate $\kappa_i(t)$ in such a way that the *steady-state* solution of the lumped model $\bar{F}_i^{\text{ss}}$ is the same with the *steady-state* solution of the distributed model F_i^{ss}, as it was done in [2, 11, 10].

For constant ω and v, the steady-state of the lumped model is found by setting $\dot{\bar{z}}_i(t) = 0$ in (46). Hence,

$$\bar{z}_i^{\text{ss}} = \frac{v_{ri}}{C_{0i}(v_r) + \kappa_i^{\text{ss}}|\omega r|}, \quad i = x, y \tag{48}$$

where κ_i^{ss} is defined by

$$\kappa_i^{\text{ss}} = -\frac{\int_0^L z_i^{\text{ss}}(\zeta) f_n'(\zeta)\mathrm{d}\zeta}{\int_0^L z_i^{\text{ss}}(\zeta) f_n(\zeta)\mathrm{d}\zeta}, \quad i = x, y \tag{49}$$

and where z_i^{ss} from (33). Calculation of κ_i^{ss} is not easy using directly the definition (49). Instead, we calculate κ_i^{ss} so that the distributed and the lumped models produce the same steady-state forces. Enforcing $F_i^{\text{ss}} = \bar{F}_i^{\text{ss}}$ $(i = x, y)$, yields

$$\bar{z}_i^{\text{ss}} = \frac{1}{F_n}\int_0^L z_i^{\text{ss}}(\zeta) f_n(\zeta)\mathrm{d}\zeta, \quad i = x, y \tag{50}$$

The explicit expression for $\bar{z}_i^{\text{ss}}$ is given in the Appendix. Once $\bar{z}_i^{\text{ss}}$ is computed from (50), $\kappa(t)$ in (46) is approximated by solving (48) for κ_i^{ss}, yielding

$$\kappa_i^{\text{ss}} = \frac{1}{|\omega r|}\left(\frac{v_{ri}}{\bar{z}_i^{\text{ss}}} - C_{0i}(v_r)\right), \quad i = x, y. \tag{51}$$

To calculate a lumped model for the aligning torque, recall first that the expression for the aligning torque along the contact patch is given from (31) and (29). Using the definition of the mean internal fiction state $\bar{z}_y$ from in (41), the expression for $M_z(t)$ can be written as follows

$$\begin{aligned} M_z(t) = \frac{L}{2}\left(\sigma_{0y}\bar{z}_y(t) + \sigma_{1y}\dot{\bar{z}}_y(t) + \sigma_{2y}v_{ry}\right) - \sigma_{0y}\int_0^L z_y(t,\zeta) f_n(\zeta)\zeta\mathrm{d}\zeta \\ + \sigma_{1y}\int_0^L \frac{\partial z_y(t,\zeta)}{\partial t} f_n(\zeta)\zeta\mathrm{d}\zeta + \sigma_{2y}v_{ry}\int_0^L f_n(\zeta)\zeta\mathrm{d}\zeta \end{aligned} \tag{52}$$

Define now the weighted mean internal state $\hat{z}_y$ for the aligning torque as follows

$$\hat{z}_y(t) := \frac{1}{F_n L}\int_0^L z_y(t,\zeta) f_n(\zeta)\zeta \mathrm{d}\zeta. \tag{53}$$

Thus,

$$\frac{\mathrm{d}\hat{z}_y(t)}{\mathrm{d}t} = \frac{1}{F_n L}\int_0^L \frac{\partial z_y(t,\zeta)}{\partial t} f_n(\zeta)\zeta \mathrm{d}\zeta. \tag{54}$$

The total aligning torque can then be written in terms of the mean states $\bar{z}_y$ and $\hat{z}_y$, as follows

$$\begin{aligned}\frac{M_z(t)}{F_n L} &= \sigma_{0y}\left(\tfrac{1}{2}\bar{z}_y(t) - \hat{z}_y(t)\right) + \sigma_{1y}\left(\tfrac{1}{2}\dot{\bar{z}}_y(t) - \dot{\hat{z}}_y(t)\right) \\ &\quad + \sigma_{2y}\left(\tfrac{1}{2}v_{ry} - \frac{G}{F_n L}\right)\end{aligned} \tag{55}$$

where,

$$G = \int_0^L f_n(\zeta)\zeta \mathrm{d}\zeta \tag{56}$$

For the case of a trapezoidal normal load distribution as in (37) we have

$$G = \frac{\alpha_1}{3}\zeta_L^3 + \frac{f_{\max}}{2}\left(\zeta_R^2 - \zeta_L^2\right) + \frac{\alpha_2}{3}\left(L^3 - \zeta_R^3\right) + \frac{\beta}{2}\left(L^2 - \zeta_R^2\right). \tag{57}$$

Finally, we need to find the dynamics of the mean state $\hat{z}_y$. Using (54) we have that

$$\begin{aligned}\dot{\hat{z}}_y(t) &= \frac{1}{F_n L}\int_0^L \frac{\partial z_y(t,\zeta)}{\partial t} f_n(\zeta)\zeta \mathrm{d}\zeta \\ &= \frac{1}{F_n L}\int_0^L \left(v_{ry} - C_{0y}(v_r) z_y(t,\zeta) - \frac{\partial z_y(t,\zeta)}{\partial \zeta}|\omega r|\right) f_n(\zeta)\zeta \mathrm{d}\zeta \\ &= \frac{G}{F_n L}v_{ry} - C_{0y}(v_r)\hat{z}_y(t) - \frac{|\omega r|}{F_n L}\int_0^L \frac{\partial z_y(t,\zeta)}{\partial \zeta} f_n(\zeta)\zeta \mathrm{d}\zeta \\ &= \frac{G}{F_n L}v_{ry} - C_{0y}(v_r)\hat{z}_y(t) - \frac{|\omega r|}{F_n L}\left[z_y(t,\zeta) f_n(\zeta)\zeta\right]_0^L \\ &\quad + \frac{|\omega r|}{F_n L}\int_0^L z_y(t,\zeta)\frac{\partial f_n}{\partial \zeta}\zeta \mathrm{d}\zeta + \frac{|\omega r|}{F_n L}\int_0^L z_y(t,\zeta) f_n(\zeta)\mathrm{d}\zeta \\ &= \frac{G}{F_n L}v_{ry} - C_{0y}(v_r)\hat{z}_y(t) - \nu(t)|\omega r|\hat{z}_y(t) + \frac{|\omega r|}{L}\bar{z}_y(t)\end{aligned} \tag{58}$$

where,

$$\nu(t) := -\frac{\int_0^L z_y(t,\zeta) f_n'(\zeta)\zeta \mathrm{d}\zeta}{\int_0^L z_y(t,\zeta) f_n(\zeta)\zeta \mathrm{d}\zeta} \tag{59}$$

where, again $(|\omega r|/(F_n L))\left[z_i(t,\zeta) f_n(\zeta)\zeta\right]_0^L = 0$ because of the assumed normal load distribution in (37). Thus, the average lumped model for the aligning torque is summarized by

$$\dot{\hat{z}}_y(t) = \frac{G}{F_n L} v_{ry} - C_{0y}(v_r)\hat{z}_y(t) - \nu(t)|\omega r|\hat{z}_y(t) + \frac{|\omega r|}{L}\bar{z}_y(t) \tag{60}$$

$$\begin{aligned}\frac{\hat{M}_z(t)}{F_n L} &= \sigma_{0y}\left(\tfrac{1}{2}\bar{z}_y(t) - \hat{z}_y(t)\right) + \sigma_{1y}\left(\tfrac{1}{2}\dot{\bar{z}}_y(t) - \dot{\hat{z}}_y(t)\right) \\ &\quad + \sigma_{2y}\left(\tfrac{1}{2}v_{ry} - \frac{G}{F_n L}\right).\end{aligned} \tag{61}$$

Notice, that by definition, $\hat{M}_z(t) = M_z(t)$. However, the calculation of $\hat{z}_y(t)$ from (60) requires knowledge of $\nu(t)$ from (59) which is not easy to obtain. Following the same reasoning as for the case of the lumped model forces, we approximate $\nu(t)$ in (60) by an appropriate constant value, ν^{ss} by assuming that, at *steady-state*, the aligning torque predicted by the lumped model $\hat{M}_z^{\text{ss}}$ will be the same with the one predicted by the distributed model M_z^{ss} given in (36).

The steady-state of the lumped model is found by setting $\dot{\hat{z}}_y = 0$, $\bar{z}_y = \bar{z}_y^{\text{ss}}$ and $\dot{\bar{z}}_y = 0$ in (61). This leads to the following expression for the steady-state $\hat{z}_y^{\text{ss}}$

$$\hat{z}_y^{\text{ss}} = \frac{1}{2\sigma_{0y}}\left(\sigma_{0y}\bar{z}_y^{\text{ss}} + \sigma_2 v_{ry}\right) - \frac{M_z^{\text{ss}}}{F_n L \sigma_{0y}} - \frac{G\sigma_2 v_{ry}}{\sigma_{0y}} \tag{62}$$

where $\bar{z}_y^{\text{ss}}$ from (50) and M_z^{ss} from (36). In order to compute ν^{ss} we let $\dot{\hat{z}}_y = 0$, $\bar{z}_y(t) = \bar{z}_y^{\text{ss}}$ and $\hat{z}_y(t) = \hat{z}_y^{\text{ss}}$ in (60) to finally obtain

$$\nu^{\text{ss}} = \frac{1}{|\omega r|}\left(\frac{1}{\hat{z}_y^{\text{ss}}}\left(\frac{G v_{ry}}{F_n L} + \frac{|\omega r|\bar{z}_y^{\text{ss}}}{L}\right) - C_{0y}\right), \tag{63}$$

where $\bar{z}_y^{\text{ss}}$ from (50) and $\hat{z}_y^{\text{ss}}$ from (62).

6 EFFECT OF STEERING ANGLE RATE

Thus far, we have derived a model that predicts the friction forces and moments at the contact patch of the wheel when the steering angle of the wheel ϕ remains constant. In order to include the effect of the angular velocity $\dot{\phi}$ of the wheel rim we first rewrite the expression for the relative velocity at the contact patch; see also Fig. 3. We thus have

$$v_{rx} = \omega r - v\cos(\alpha) \tag{64a}$$

$$v_{ry}(\zeta) = -v\sin(\alpha) - \left(\frac{L}{2} - \zeta\right)\dot{\phi} \tag{64b}$$

Observe that in this case the relative velocity v_{ry} is a function of the position on the contact patch ζ. The new definition of the relative velocity v_{rx} and v_{ry} can be used in the distributed model (29)-(31) to calculate the friction forces and moments at the contact patch including the effect of $\dot{\phi}$. However, since now v_{ry} depends on ζ the dynamics of the lumped model (44) and (58) are not valid anymore. In order to include the effect of $\dot{\phi}$ on the *average lumped* model we propose in this section a LuGre-type dynamic friction model for the angular motion of the wheel about an axis normal to the contact area.

Consider as in Fig. 9 the rotation of a wheel about an axis normal to the contact patch. Let, in analogy to Section 3, assume that the forces developed

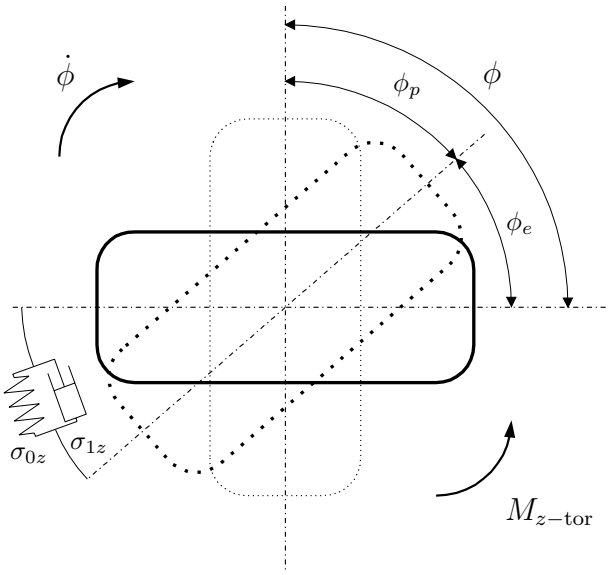

Figure 9: Angular motion of the contact patch.

due to this rotation are due to microscopic *torsional* springs/bristles in the contact patch. Assume also that ϕ_p is the plastic angular deformation and ϕ_e the elastic angular deformation of these bristles. Let $\phi = \phi_p + \phi_e$ be the total angle of rotation. Denote by $M_{z-\mathrm{tor}}$ the friction moment due to the relative rotation of the wheel with respect to the surface and let

$$\mu_{z-\mathrm{tor}} := \frac{M_{z-\mathrm{tor}}}{F_n L} \tag{65}$$

the associated torsional friction coefficient. Let also μ_{kz} be the asymptotic (as $\dot{\phi} \to \infty$) friction moment coefficient and $k_z = F_n L \sigma_{0z}$ the torsional stiffness.

The elastic and plastic angular deformations are $\phi_e = -k_z^{-1} F_n L \mu_{z-\mathrm{tor}}$ and $\phi_p = \phi - \phi_e$ respectively. The dissipation rate associated to the friction moment

is $D(\dot{\phi}_p, \mu_{z-\mathrm{tor}}) = -F_n L \mu_{z-\mathrm{tor}} \dot{\phi}_p$. Following the same reasoning as in the case of the 2D motion in Sections 3 and 4, we find the torsional friction coefficient by solving an associated QVI. We then derive to the following dynamic LuGre-type friction model for the angular relative motion of the wheel with respect to the contact area

$$\dot{z}_z(t) = \dot{\phi} - \frac{\sigma_{0z}|\dot{\phi}|}{g_z(\dot{\phi})} z_z(t) \tag{66a}$$

$$g_z(\dot{\phi}) = \mu_{kz} + (\mu_{sz} - \mu_{kz})\, e^{-\left(\frac{\dot{\phi}}{\dot{\phi}_s}\right)^{\beta}} \tag{66b}$$

and

$$M_{z-\mathrm{tor}} = -F_n L \left(\sigma_{0z} z_z + \sigma_{1z} \dot{z}_z + \sigma_{2z} \dot{\phi}\right) \tag{67}$$

This model can be used to include the effect of $\dot{\phi}$ to the moment predicted by the lumped model (44), (58) and (55). The total moment predicted by the average lumped model will then be the summation of $M_{z-\mathrm{tor}}$ and M_z from (55) where the latter is computed using the initial definition of the relative velocity (28) without the $\dot{\phi}$ term,

$$M_{z-\mathrm{total}} = M_z + M_{z-\mathrm{tor}}. \tag{68}$$

There is a final point that requires further clarification. It is not only the aligning torque that needs adjustment when we include the effects of the wheel rim rotation. Since the expression of v_{ry} depends on ζ, there should be some adjustment to the lateral forces as well. To simplify the model, we have assumed that the rotation of the rim does not affect the longitudinal and lateral friction forces, and that the definition (28) can still be used for the relative velocity. This is a realistic assumption, since in relatively high speeds the term $\left(\frac{L}{2} - \zeta\right)\dot{\phi}$ is much smaller compared to $v\sin(\alpha)$ due to the small length of the patch and the relatively small steering velocity $\dot{\phi}$. Furthermore, in small vehicle velocities the normal load distribution is closer to a symmetric one. Considering only the rotation of the wheel rim $\dot{\phi}$ and the symmetry of the normal load distribution results in cancellation of the lateral friction forces. This is demonstrated in the next section.

In conclusion, we emphasize that the introduction of equations (66)-(67) to the average lumped tire model has been done rather artificially. As mentioned earlier, the effect of $\dot{\phi}$ is captured by the distributed model (29)-(31) by introducing the definition (64) and without adding any new parameters to the system. In order for the *average lumped* model to capture the effect of $\dot{\phi}$ we introduced equations (66)-(67) and a new set of parameters σ_{0z}, σ_{1z}, σ_{2z}, μ_{kz}, μ_{sz}, $\dot{\phi}_s$ and β. The coefficients of (66)-(67) can be identified by comparing the distributed and the lumped models.

Next, we propose a steady-state scenario ($v = 0$, $\omega = 0$ and $\dot{\phi} \neq 0$) in order to predict the torsional torque of the distributed model, and then identify the remaining coefficients in such a way, that the behavior of the lumped model captures the behavior of the distributed one at steady-state. Note that for the

case $v = \omega = 0$, $\dot{\phi} \neq 0$ the self-aligning torque is zero and the only moment acting normal to the patch is the torsional moment.

6.1 Identification of the Torsional Equation Parameters

In this section we identify the parameters of the torsional equations (66)-(67) of the average lumped model by comparing it with the distributed model using a special steady-state case scenario. In particular, consider the case when $\omega, v = 0$ and $\dot{\phi} = \text{const}$. The relative velocity v_r is then

$$\begin{aligned} v_{rx} &= 0 \\ v_{ry} &= -\dot{\phi}\left(\frac{L}{2} - \zeta\right). \end{aligned} \tag{69}$$

In this particular case, and since $\omega = 0$, the equations of the internal friction states from the distributed model reduce to

$$\frac{\partial z_i}{\partial t} + \frac{\partial z_i}{\partial \zeta}|\omega r| = \frac{\partial z_i}{\partial t} = v_{ri} - C_{0i}(v_r) z_i \tag{70}$$

where $i = x, y$. Also, in steady-state, we have $\frac{\partial z_i}{\partial t} = 0$ which leads to the following steady-state values

$$z_i^{\text{ss}} = \frac{v_{ri}}{C_{0i}(v_r)}, \qquad i = x, y \tag{71}$$

Obviously, and since $v_{rx} = 0$, we have $z_x^{\text{ss}} = 0$ and the steady-state longitudinal force is $F_x^{\text{ss}} = 0$.

As far as the value of z_y^{ss} is concerned, imposing $v_{rx} = 0$, we have from (18), (27) and (71),

$$z_y^{\text{ss}} = \text{sign}(v_{ry}) \frac{g(v_{ry})}{\sigma_{0y}}. \tag{72}$$

Now observe that for $v_{rx} = 0$ the function $g(v_{ry})$ in (23) becomes

$$g(v_{ry}) = \mu_{ky} + (\mu_{sy} - \mu_{ky}) \exp\left[-\left(\frac{|\dot{\phi}|\,|L/2 - \zeta|}{v_s}\right)^{\gamma}\right] \tag{73}$$

At this point we make one final assumption. Since $v = 0$, it is necessary to assume a symmetric normal load distribution that will impose symmetry in the friction forces. For simplicity, we choose $f_n = F_n/L = \text{const}$. Recall that

$$\mu_y^{\text{ss}} = -\sigma_{0y} z_y^{\text{ss}} - \sigma_{2y} v_{ry} \tag{74}$$

Since z_y^{ss} is symmetric with respect to the center of the patch (Fig. 10), and assuming a uniform load distribution, we conclude that the lateral forces cancel each other out, resulting in $F_y^{\text{ss}} = 0$.

The total moment predicted by the distributed model (31) in case when $\omega, v = 0$ and $\dot{\phi} = \text{const.}$ is given by

$$M_{z-\text{total}}^{\text{ss}} = -\text{sign}(\dot{\phi})\frac{1}{4}\mu_{ky} f_n L^2 - 2\frac{(\mu_{sy} - \mu_{ky}) f_n v_s}{\dot{\phi}} \left(-\frac{L}{2} e^{-\frac{L|\dot{\phi}|}{2v_s}} + \frac{v_s}{|\dot{\phi}|}(1 - e^{-\frac{L|\dot{\phi}|}{2v_s}}) \right) \tag{75}$$

Since there is no self-aligning torque in case when $\omega, v = 0$ this equation gives also the value of the torsional moment in (68). Comparing (75) with the steady-state torsional component of the lumped model (66)-(67) given by

$$z_z^{\text{ss}} = \text{sign}(\dot{\phi})\frac{g_z(\dot{\phi})}{\sigma_{0z}} \tag{76a}$$

$$M_{z-\text{tor}}^{\text{ss}} = -F_n L \left(\sigma_{0z} z_z^{\text{ss}} + \sigma_{2z}\dot{\phi} \right) \tag{76b}$$

we can identify the parameters $\mu_{sz}, \mu_{kz}, \dot{\phi}_s, \sigma_{2z}$ and β. For different values of $\dot{\phi}$ we have identified the parameters $\mu_{sz}, \mu_{kz}, \dot{\phi}_s, \sigma_{2z}$ and β by comparing the plots generated by the distributed model steady state (75) with the plots generated by the average lumped model steady state (76). The parameters identified using this approach are shown in the following table, and the result of the curve fitting is shown in Fig. 10.

Table 3: Identified Parameters

μ_{kz}	μ_{sz}	σ_{2z}	$\dot{\phi}_s$(rad/sec)	β
0.76	0.91	0	74	1

7 DYNAMIC RESPONSE OF THE MODEL

Comparison of the transient response of the longitudinal lumped LuGre tire friction model with experimental data have been reported in [11]. Validating the combined longitudinal/lateral behavior of the model is not as straightforward. In fact, experimental results for combined longitudinal/lateral behavior of tire models under realistic transient conditions are scarce in the literature. In this section we present a validation of the dynamic response of the tire friction for the combined longitudinal/lateral motion predicted by the proposed model against the results found in [9]. Specifically, we compare the responses of our model to the ones in [9] under similar excitations.

In [9] a static map of relative velocity to friction and the dynamics of slip and slip angle development are used to predict tire friction forces by taking into consideration the effects of relaxation length. Experimental results using a "Mobile Tire Tester" are presented for different braking inputs. The "Mobile

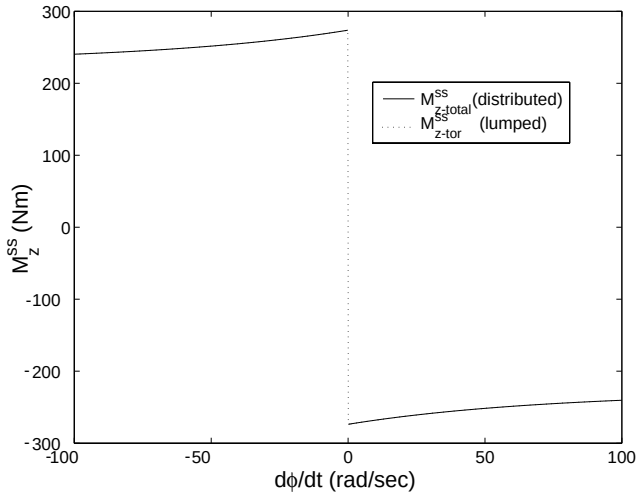

Figure 10: Comparison between $M^{\rm ss}_{z-{\rm tor}}$ and $M^{\rm ss}_{z-{\rm total}}$ from data fitting; case when $v = \omega = 0$.

Tire Tester" is an experimental test-bed that allows independent control of slip angle, rate of rotation and travel velocity of a tire. Both experimental and simulation results are given in [9] corresponding to a case of constant travel speed and slip angle and with different braking profiles which affect only the wheel's rotation rate.

Similar simulations have been conducted with the model developed in this paper using linearly increasing and "stair-step" increasing braking torques under constant vehicle speed ($v = 8$ m/sec) and wheel slip angle ($\alpha = 4$ deg) as in [9]. The dynamic response of the friction forces (Fig. 11) is in complete accordance with the results given in [9]. In particular, it is verified that the longitudinal and lateral force components predicted when longitudinal slip is increasing are considerably different from those predicted when slip is decreasing rapidly (first column of Fig. 11, linear increase of braking torque). This implies that dynamic effects may not be neglected. We also observe the same patterns in friction development due to steps in torque (second column of Fig. 11, "stair-step" increase of braking torque) as might be introduced by a poor anti-lock braking system or a jerky driver as mentioned in [9]. These results are in agreement with the experimental observations in [9]. Notice in particular the hysteretic loops in bottom two rows of Fig. 11. These loops are exclusively a dynamic phenomenon and cannot be reproduced by steady-state models.

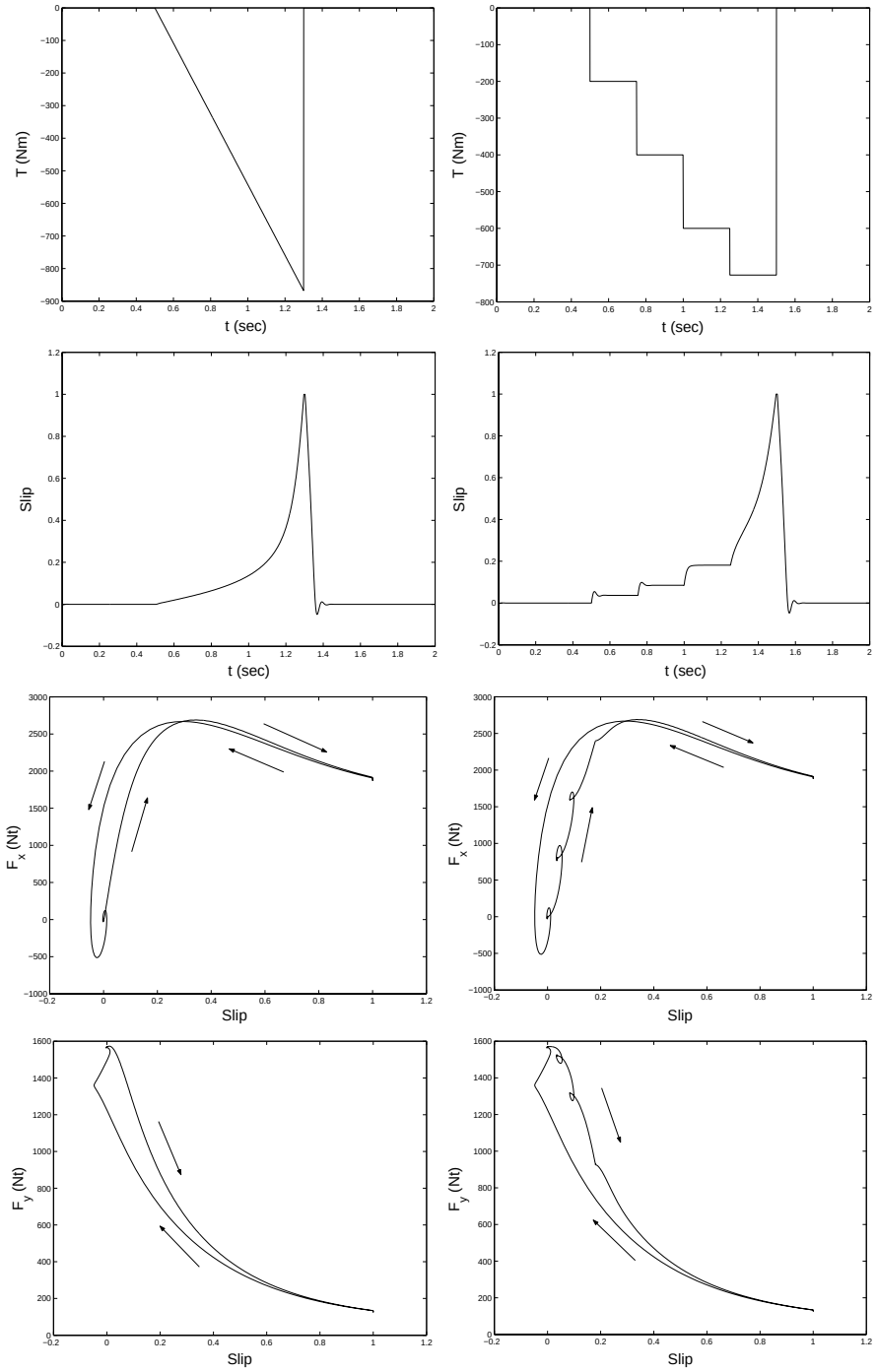

Figure 11: Dynamic response of friction for linear (left column) and "stair-step" increasing (right column) braking torque. The results are in complete agreement with those presented in [9].

8 CONCLUSIONS

An extension of the LuGre dynamic tire friction model from longitudinal to the combined longitudinal/lateral motion has been presented. This 3-dof model, is derived from first principles, by applying the LuGre *point* friction model to the tire/ground interface. The model proposed captures the anisotropy of the static friction characteristics. The dynamic nature of the model overcomes discrepancies and singularities of slip-based static friction models. In order to obtain as a simple model as possible (i.e. with as a small number of states as possible) to allow on-line control and estimation, a lumped model is introduced to avoid dealing with partial differential equations. The lumped model ensures that the friction forces and aligning torque are the same as the ones predicted by the distributed model, at least at steady-state. The effects of the steering angle rate can be taken into account for small vehicle velocities by adding the effect of wheel steer via an additional LuGre-type model having as input the steering wheel velocity. Simulations have been presented that validate the success of the model in predicting qualitatively and quantitatively both the dynamic and steady state characteristics of tire friction. The fidelity of the model can be increased, if needed, by including additional dynamics such as camber, dynamic normal force distribution, belt deflection etc. The price to pay, of course, is increased model complexity.

ACKNOWLEDGEMENTS

This work was partially supported by NSF (award No. INT-9726621/INT-9996096). The work of the first two authors was also supported by the US Army Research Office (contract No. DAAD19-00-1-0473).

REFERENCES

1. J. Szymansky, "Modèles réduits du contact pneu-sol et applications à l'automobile," Technical Report, Renault, Technocentre Renault, Guyancourt, France, 1999.
2. J. Deur, "Modeling and analysis of longitudinal tire dynamics based on the LuGre friction model," Technical Report, Ford Motor Company, Scientific Research Laboratory MD 1170, Dearborn, MI 48121-2053, USA, 2001.
3. X. Claeys, C. Canudas de Wit, J. Yi, R. Horowitz, L. Alvarez, and L. Richard, "A new 3d dynamic tire/road friction model for vehicle simulation and control," in *Proceedings of the ASME-IMECE World Conference*, (New York, USA), November 2001.
4. E. Bakker, L. Nyborg, and H. Pacejka, "Tyre modelling for use in vehicle dynamics studies," *SAE paper # 870421*, 1987.
5. H. Pacejka and E. Bakker, "The magic formula tyre model," in *Proceedings of 1st International Colloquium on Tyre Models for Vehicle Dynamics Analysis*, (Delft, The Netherlands), October 21-22, 1991.

6. P. Bliman and M. Sorine, "A system-theoretic approach of systems with hysteresis application to friction modelling and compensation," in *Proceedings of 2nd European Control Conference*, (Gröningen, The Netherlands), 1993.
7. P. Bliman, T. Bonald, and M. Sorine, "Hysteresis operators and tyre friction models. application to vehicle dynamic simulation," in *Proceedings of ICIAM 95*, (Hamburg, Germany), July 3-7, 1995.
8. M. Sorine and J. Szymanski, "A new dynamic multi d.o.f. tire model," in *Transportation Systems 2000*, (Braunschweig, Germany), 2000.
9. P. Fancher, J. Bernard, C. Clover, and C. Winkler, "Representing truck tire characteristics in simulations of braking and braking-in-a-turn maneuvers," *Vehicle System Dynamics Supplement*, vol. 27, pp. 207–220, 1997.
10. J. Deur, J. Asgari, and D. Hrovat, "A dynamic tire friction model for combined longitudinal and lateral motion," in *Proceedings of the ASME-IMECE World Conference*, (New York, USA), November 2001.
11. C. Canudas de Wit, P. Tsiotras, E. Velenis, M. Basset, and G. Gissinger, "Dynamic friction models for road/tire longitudinal interaction," *Vehicle System Dynamics*, vol. 39, no. 3, pp. 189–226, 2003.
12. P. Bliman and M. Sorine, "Easy-to-use realistic dry friction models for automatic control," in *Proceedings of 3rd European Control Conference*, (Rome, Italy), pp. 3788–3794, September, 1995.
13. C. Canudas de Wit and P. Tsiotras, "Dynamic tire friction models for vehicle traction control," in *Proceedings of 38th IEEE Conference on Decision and Control*, (Phoenix, Arizona, USA), pp. 3746–3751, 1999.
14. C. Canudas de Wit, H. Olsson, K. J. Åström, and P. Lischinsky, "A new model for control of systems with friction," *IEEE Transactions on Automatic Control*, vol. 40, no. 3, pp. 419–425, 1995.
15. C. Canudas-de Wit, M. Petersen, and A. Shiriaev, "A new nonlinear observer for tire/road distributed contact friction," in *Proceedings of the* 42^{th} *IEEE Conference on Decision and Control*, December 9-12 2003. Maui, Hawaii, to appear.
16. C. Canudas de Wit, R. Horowitz, and P. Tsiotras, "Model-based observers for tire/road contact friction prediction," in *New Directions in Nonlinear Observer Design* (H. Nijmeijer and T. Fossen, eds.), vol. 244 of *Lecture Notes in Control and Information Science*, pp. 23–42, London: Springer-Verlag, 1999.
17. C. Canudas de Wit and P. Tsiotras, "Dynamic tire friction models for vehicle traction control," in *38th IEEE Conference on Decision and Control*, pp. 3746–3751, 1999. Phoenix, AZ.
18. M. Sorine, "Applications of hysteresis models: Contact friction in tires, muscle contraction," in *IEEE CDC 98 Workshop #2*, (Tampa, Florida), 1998.
19. J. Wong, *Theory of Ground Vehicles*. New York: John Wiley and Sons, Inc., 1978.
20. D. Casanova, R. S. Sharp, and P. Symonds, "Minimum time manoeuvring: The significance of yaw inertia," *Vehicle System Dynamics*, vol. 34, pp. 77–115, 2000.
21. J. Hendrikx, T. Meijlink, and R. Kriens, "Application of optimal control theory to inverse simulation of car handling," *Vehicle System Dynamics*, vol. 26, pp. 449–461, 1996.
22. R. S. Sharp, D. Casanova, and P. Symonds, "A mathematical model for driver steering control, with design, tuning and performance results," *Vehicle System Dynamics*, vol. 33, pp. 289–326, 2000.
23. E. Lim and J. Hedrick, "Lateral and longitudinal vehicle control coupling for automated vehicle operation," in *Proceedings of the American Control Conference*, June 2-4 1999. San Diego, CA.
24. J. Ackermann, J. Guldner, W. Sienel, R. Steinhauser, and V. Utkin, "Linear and nonlinear controller design for robust automatic steering," *IEEE Transactions on Control Systems Technology*, vol. 3, no. 1, pp. 132–143, 1995.
25. J. Zhang, S. Xu, and A. Rachid, "Path tracking control of vehicles based on lyapunov approach," in *Proceedings of the American Control Conference*, May 8-10 2002. Anchorage, AK.

APPENDIX: DISTRIBUTED STEADY-STATE FORCE AND MOMENT CALCULATION

Using the solution $z_i^{\mathrm{ss}}(\zeta)$ of the internal friction state $z_i(t,\zeta)$ in steady-state from (33), along with the expressions (35) and (36) for the steady-state forces and moment and equation (37) for the normal load distribution, the following expressions for the distributed steady-state forces and moment of the distributed model can be calculated.
The steady-state forces are:

$$\begin{aligned}
F_i^{\mathrm{ss}} = &-\sigma_{0i}C_{1i}\alpha_1\left(\frac{\zeta_L^2}{2}+C_{2i}\zeta_L e^{-\frac{\zeta_L}{C_{2i}}}-C_{2i}^2\left(1-e^{-\frac{\zeta_L}{C_{2i}}}\right)\right)\\
&-\sigma_{0i}C_{1i}f_{\max}\left((\zeta_R-\zeta_L)+C_{2i}\left(e^{-\frac{\zeta_R}{C_{2i}}}-e^{-\frac{\zeta_L}{C_{2i}}}\right)\right)\\
&-\frac{1}{2}\sigma_{0i}C_{1i}\alpha_2\left(L^2-\zeta_R^2\right)-\sigma_{0i}C_{1i}\beta_2\left(L-\zeta_R\right)\\
&-\sigma_{0i}C_{1i}\alpha_2C_{2i}\left(Le^{-\frac{L}{C_{2i}}}-\zeta_R e^{-\frac{\zeta_R}{C_{2i}}}\right)\\
&-\sigma_{0i}C_{1i}C_{2i}\left(\beta_2+\alpha_2C_{2i}\right)\left(e^{-\frac{L}{C_{2i}}}-e^{-\frac{\zeta_R}{C_{2i}}}\right)\\
&-\sigma_{2i}v_{ri}\left(\frac{1}{2}\alpha_1\zeta_L^2+f_{\max}\left(\zeta_R-\zeta_L\right)+\frac{1}{2}\alpha_2\left(L^2-\zeta_R^2\right)+\beta_2\left(L-\zeta_R\right)\right),\qquad i=x,y
\end{aligned}$$

The steady-state aligning torque is:

$$\begin{aligned}
M_z^{\mathrm{ss}} = &\sigma_{0y}C_{1y}\alpha_1\zeta_L^2\left(\frac{L}{4}-\frac{\zeta_L}{3}\right)+\frac{1}{2}\sigma_{0y}C_{1y}\alpha_1LC_{2y}\left(\zeta_L e^{-\frac{\zeta_L}{C_{2y}}}+C_{2y}e^{-\frac{\zeta_L}{C_{2y}}}-C_{2y}\right)\\
&+\sigma_{0y}C_{1y}\alpha_1C_{2y}\left(-\zeta_L^2e^{-\frac{\zeta_L}{C_{2y}}}-2C_{2y}\zeta_L e^{-\frac{\zeta_L}{C_{2y}}}-2C_{2y}^2\left(e^{-\frac{\zeta_L}{C_{2y}}}-1\right)\right)\\
&+\sigma_{0y}C_{1y}f_{\max}\left(\frac{L}{2}\left(\zeta_R-\zeta_L\right)-\frac{1}{2}\left(\zeta_R^2-\zeta_L^2\right)+\frac{L}{2}C_{2y}\left(e^{-\frac{\zeta_R}{C_{2y}}}-e^{-\frac{\zeta_L}{C_{2y}}}\right)\right)\\
&+\sigma_{0y}C_{1y}f_{\max}C_{2y}\left(-\zeta_R e^{-\frac{\zeta_R}{C_{2y}}}+\zeta_L e^{-\frac{\zeta_L}{C_{2y}}}-C_{2y}\left(e^{-\frac{\zeta_R}{C_{2y}}}-e^{-\frac{\zeta_L}{C_{2y}}}\right)\right)\\
&+\sigma_{0y}C_{1y}\alpha_2\left(\frac{L}{4}\left(L^2-\zeta_R^2\right)-\frac{1}{3}\left(L^3-\zeta_R^3\right)\right)+\sigma_{0y}C_{1y}\beta_2\left(\frac{L}{2}\left(L-\zeta_R\right)-\frac{1}{2}\left(L^2-\zeta_R^2\right)\right)\\
&+\frac{1}{2}\sigma_{0y}C_{1y}\alpha_2LC_{2y}\left(Le^{-\frac{L}{C_{2y}}}-\zeta_R e^{-\frac{\zeta_R}{C_{2y}}}+C_{2y}\left(e^{-\frac{L}{C_{2y}}}-e^{-\frac{\zeta_R}{C_{2y}}}\right)\right)\\
&+\sigma_{0y}C_{1y}\beta_2C_{2y}\left(-Le^{-\frac{L}{C_{2y}}}+\zeta_R e^{-\frac{\zeta_R}{C_{2y}}}-C_{2y}\left(e^{-\frac{L}{C_{2y}}}-e^{-\frac{\zeta_R}{C_{2y}}}\right)\right)\\
&+\frac{1}{2}\sigma_{0y}C_{1y}\beta_2LC_{2y}\left(e^{-\frac{L}{C_{2y}}}-e^{-\frac{\zeta_R}{C_{2y}}}\right)+\sigma_{0y}C_{1y}\alpha_2C_{2y}\left(-L^2e^{-\frac{L}{C_{2y}}}+\zeta_R^2e^{-\frac{\zeta_R}{C_{2y}}}\right)\\
&+2\sigma_{0y}C_{1y}\alpha_2C_{2y}^2\left(-Le^{-\frac{L}{C_{2y}}}+\zeta_R e^{-\frac{\zeta_R}{C_{2y}}}-C_{2y}\left(e^{-\frac{L}{C_{2y}}}-e^{-\frac{\zeta_R}{C_{2y}}}\right)\right)
\end{aligned}$$

$$+\sigma_{2y}v_{ry}\alpha_1\zeta_L^2\left(\frac{L}{4}-\frac{\zeta_L}{3}\right)+\frac{1}{2}\sigma_{2y}v_{ry}f_{\max}\left(L\zeta_R-L\zeta_L-\zeta_R^2+\zeta_L^2\right)$$
$$+\sigma_{2y}v_{ry}\alpha_2\left(\frac{L}{4}\left(L^2-\zeta_R^2\right)-\frac{1}{3}\left(L^3-\zeta_R^3\right)\right)+\sigma_{2y}v_{ry}\beta_2\left(\frac{L}{2}\left(L-\zeta_R\right)-\frac{1}{2}\left(L^2-\zeta_R^2\right)\right)$$

Similarly, the expression for $\bar{z}_i^{\text{ss}}$ is computed from (50) as follows

$$\begin{aligned}\bar{z}_i^{\text{ss}}=&\frac{1}{F_n}C_{1i}\alpha_1\left(\frac{\zeta_L^2}{2}+C_{2i}\zeta_L e^{-\frac{\zeta_L}{C_{2i}}}-C_{2i}^2\left(1-e^{-\frac{\zeta_L}{C_{2i}}}\right)\right)\\&+\frac{1}{F_n}C_{1i}f_{\max}\left(\left(\zeta_R-\zeta_L\right)+C_{2i}\left(e^{-\frac{\zeta_R}{C_{2i}}}-e^{-\frac{\zeta_L}{C_{2i}}}\right)\right)\\&+\frac{1}{2}\frac{1}{F_n}C_{1i}\alpha_2\left(L^2-\zeta_R^2\right)+\frac{1}{F_n}C_{1i}\beta_2\left(L-\zeta_R\right)\\&+\frac{1}{F_n}C_{1i}\alpha_2C_{2i}\left(Le^{-\frac{L}{C_{2i}}}-\zeta_R e^{-\frac{\zeta_R}{C_{2i}}}\right)\\&+\frac{1}{F_n}C_{1i}C_{2i}\left(\beta_2+\alpha_2C_{2i}\right)\left(e^{-\frac{L}{C_{2i}}}-e^{-\frac{\zeta_R}{C_{2i}}}\right),\qquad i=x,y\end{aligned}$$

These expressions were used to construct the steady-state plots of Fig. 5, Fig. 6 and Fig. 7, as well as in the parameter identification of Section 5.3.